Numerical Prediction of Ingestion Mass Flow Rate on Hall Thruster Performance Measurement

IEPC-2017- 340

Presented at the 35th International Electric Propulsion Conference
Georgia Institute of Technology • Atlanta, Georgia • USA
October 8 – 12, 2017

Gen Ito[1] [2]
IHI Corporation, Yokohama, Kanagawa, 235-8501, Japan
The University of Tokyo, Hongo, Tokyo, 113-8654, Japan

Rei Kawashima[3], Kimiya Komurasaki[4] and Hiroyuki Koizumi[5]
The University of Tokyo, Hongo, Tokyo, 113-8654, Japan

and

Kenji Fuchigami[6]
IHI Corporation, Yokohama, Kanagawa, 235-8501, Japan

Abstract: Numerical simulation to predict the facility background flow effects on Hal thruster performance measurement has been developed. Ingestion particles were counted by Direct Simulation Monte Carlo method. It was revealed that the particles inside the vacuum chamber reflected more than ten times at chamber wall and pumps. The pump sticking coefficient is currently one of the tuning parameter in the other estimation methods of the ingestion mass flow rate and pressure distribution inside the vacuum chamber. In order to increase the reliability, pump sticking coefficient of a cryopump was analytically estimated. The validation of the estimated pump sticking coefficient was conducted by comparing pressure distribution estimated by numerical simulation and measured by experiment. The simulation result agrees with the measured result within the range of measurement error. Three-dimensional simulation of the particle motion inside the φ 3 m × 9 m vacuum chamber was conducted by using estimated pump sticking coefficient. By counting the particles to the thruster discharge chamber, ingestion mass flow rate during the performance test of 600 mN class Hall-thruster was estimated. The investigation of the relationship between target shape and the estimated ingestion mass flow rate show that the conical target is able to reduce the ingestion mass flow when the particles motion is able to be treated as collision-less.

Nomenclature

A	=	area of the cell boundary
d_{btb}	=	distance of the baffle to baffle in the first stage of cryopump
d_c	=	distance between outer discharge chamber and inner discharge chamber

[1] Researcher, Research Laboratory, gen_ito@ihi.co.jp.
[2] Doctoral student, Department of Aeronautics and Astronautics, g.ito@al.t.u-tokyo.ac.jp.
[3] Research Associate, Department of Aeronautics and Astronautics, kawashima@al.t.u-tokyo.ac.jp.
[4] Professor, Department of Aeronautics and Astronautics, komurasaki@al.t.u-tokyo.ac.jp.
[5] Associate Professor, Department of Aeronautics and Astronautics, koizumi@al.t.u-tokyo.ac.jp.
[6] Senior Researcher, Research Laboratory, kenji_fuchigami@ihi.co.jp.

d_{oc} = diameter of the outer discharge chamber of Hall thruster
F = flux of the flow
i = cell boundary index
h_p = height of cryopump
h_{1st} = height of the first stage baffle of cryopump
h_{2st} = height of the second stage of cryopump
k_B = Boltzmann's constant
m_a = anode mass flow rate
n_n = number density inside the neutralizer
P_{+x} = total pressure of the plus x direction
P_c = corrected facility pressure
P_b = base facility pressure
r_p = radius of the side wall of cryopump
r_{1st} = radius of the first stage baffle of cryopump
r_{2st} = radius of the second stage of cryopump
V_a = acceleration voltage
T_w = temperature of the chamber wall
w_c = width of the discharge chamber of Hall thruster
α = pump sticking coefficient
θ_{1st} = angle of the first stage baffle of cryopump
θ_{ta} = angle of the conical target
Φ_{into_n} = flux number density of the flow into the neutralizer

I. Introduction

Stationary satellite bus with large power consumption (25 kW class) is required in response to the increase in the capacity of communication and the number of channels due to the global broadband transmission of communication and broadcasting satellites. Electric power that can be used for the propulsion system also increases, and then all-electrified satellites equipped with electric propulsion have received a lot of attention for the purpose of increasing the payload. In the US, Boeing has introduced the all-electric satellite bus "702SP" to the market, and in Europe "Electra" has been developed as all-electric satellite bus in the Advanced Research in Telecommunications Systems (ARTES) program by the European Space Agency (ESA). Also in Japan, in April 2017, Mitsubishi Electric Corporation announced that they started designing an all electrified satellite bus in Engineering Test Satellite 9 (ETS-9) project by the Japan Aerospace Exploration Agency (JAXA).[1] Generating up to 25 kW of power and using Japan-made 6kW high-power Hall thrusters for its propulsion system is planned.

Recently, several high-power Hall thrusters have been developed in Japan because of this increasing demand for electric propulsion.[2] The 5 kW class anode layer type (TAL) Hall thruster RAIJIN94 and 2 kW class TAL Hall thruster UT-58 has been developed and investigated in the Robust Anode-layer Intelligent Thruster for the Japanese IN-space propulsion system (RAIJIN) project which is comprised of nine universities and JAXA.[3] Tests of RAIJIN94 were conducted in the ion engine endurance test vacuum chamber at the Institute of Space and Astronautical Science (ISAS) in JAXA. The chamber is 2 m in diameter by 5 m length, evacuated by four ULVAC CRYO-U30H cryogenic pumps (44,000 l/s for xenon), with the pressure kept below 6.6×10^{-3} Pa (for xenon) during thruster operation, with total mass flow rates of 13.5 mg/s. Tests of UT-58 were conducted in the vacuum chamber at the University of Tokyo. The chamber is 2 m in diameter by 3 m length, evacuated by one ULVAC PFL-36 oil diffusion pump (34,000 l/s). On the other hand, 2–6 kW class magnetic layer type with dual mode operation Hall thruster has been developed by JAXA, IHI, IHI Aerospace Engineering Corporation (IA), and Tokyo Metropolitan University (TMU).[2,4] For the requirements of the both high-thrust and high-I_{sp} modes, its design is aiming to put the ion production region at the appropriate downstream position. The tests campaign have been performed in three different facilities, Vacuum Test Facility 2 (VTF-2) at the Georgia Institute of Technology High-Power Electric Propulsion Laboratory (HPEPL), ISAS vacuum chamber and IHI vacuum chamber. VTF-2 is 4.9 m in diameter by 9.2 m length, evacuated by ten liquid-nitrogen-cooled CVI TMI-1200i cryogenic pumps (350,000 l/s for xenon).[5] IHI vacuum chamber is 2 m in diameter by 3 m length, evacuated by two cryogenic pumps (21,000 l/s for xenon). Utilizing the data series obtained at several different facilities is strongly required in these projects. It is essential to clarify the influence of the facility to thruster performance and operation, the so-called facility effect.

In recent years, the facility effect is considered including two major factors of electrical interaction and background pressure,[6,7] and it is necessary to investigate them separately. Background pressure is one of the primary facility

effects well studied to influence ground test results.[8-10] The artificial change of the thrust and performance of thrusters have been observed in several thrusters.[11-13] The ingestion of background neutrals presenting in the vacuum facility is considered as the cause of this phenomena. In order to predict the ingestion mass flow rate, bulk background flow modeling have been discussed by Cai and Frieman et al.[14,15] Since the propellant exhausted as accelerated plasma from electric propulsions is neutralized and reflects on the chamber wall until it is pumped out, factors related to chamber configuration should be considered in addition to the background pressure. Three-dimensional simulation is required to predict more realistically. Nakayama and Nakamura developed three-dimensional simulation using Direct Simulation Monte Carlo (DSMC) method.[16] However, there are several tuning parameters such as pump sticking coefficient and reflection condition of the particles on the walls. In order o establish the transportable simulation tool, suitable model should be decided based on physics inside the chamber. In this study, not only pressure distribution but also motion of neutral particle in vacuum chamber is focused on. At first, pump sticking coefficient was analytically estimated by using Test Particle Monte Carlo (TPMC) method which non-collisional free motion is considered. Second, using the obtained pump sticking coefficient, we developed DSMC code to analyze the motion of particles in the three-dimensional vacuum chamber. By simulating and measuring pressure distribution inside the IHI vacuum chamber, calculated pump sticking coefficient was validated. Finally, we conducted the prediction of the ingestion mass flow rate of the 600 mN class Hall thruster operation in the large vacuum chamber and investigated the influence of the target shape.

II. Cryopump analysis

A. 2D3V simulation model of the axisymmetric cryopump

The cryopump is a pump that places a cryogenic surface in a vacuum vessel and condenses or adsorbs gas molecules in the vessel to capture and exhaust them. Since there are less mechanical moving parts and oil are not used, it is possible to create a clean high vacuum. A typical cryopump consists of a cryogenic refrigerator producing refrigeration at two temperature stages. The first stage of the refrigerator usually operates around 80 K and is used to cool the outer cryopanel and baffles across the inlet opening of the cryopump. Water vapor freezes out onto these panels, but noble gases such as xenon that is widely used as propellants of electric propulsion are not frozen. The second stage operates around 10 to 20 K and is used to cool the inner cryopanels. Xenon reaching the surface of the second stage is frozen almost 100 % as long as the temperature of the stage is maintained within a range not exceeding 20 K significantly. Thus, the pump sticking coefficient α can be regarded as the ratio of the particles that passed through the first stage and reached at the second stage.

Here, axisymmetric cryopump model with two stages was assumed as shown in Fig. 1. Simulation was conducted on two dimensional Cartesian coordinate and three-dimensional components of velocity were calculated. When calculating the reflection of particles, the coordinates of the velocity were converted to cylindrical coordinates. In this simulation, the radius of the cryopump r_p was set to 0.35 m. Cryopumps are installed to pipe with gate valve at some facilities to accelerate the regeneration. Therefore, an extra cylindrical space is installed upstream of the cryopump, and this area needs to be included in the calculation of the chamber or considered as the area of the cryopump. In order to take into account such pipe, two cases with different height of the cryopump h_p, 0.40 m and 0.75 m were simulated. The first stage consists of baffles cooled to 80 K, the number of baffles vary depending on the pump. In this case, twelve baffles were assumed. The angle of the baffle was set to 36.87 degrees. Height of the baffles of the first stage h_{1st} was 0.35 m, radius of the inner baffle of the first stage r_{1st} was 0.03 m and distance of each baffles d_{btb} was 0.025 m, respectively. The second stage consists of the baffles cooled to 15 K and an adsorption tower. The height of the second stage h_{2st} was 0.025 m and the radius r_{2nd} was 0.02 m.

Particles that hit the second stage are completely frozen, i.e. excluded from the calculation. Particles that go back to the entrance of the pump were also excluded from the simulation. Particles flow from upper boundary on the model. Xenon particles that hit the wall surface or the first stage baffles were diffused without frozen and thermally accommodate. It was assumed that particles are only neutrals. Non-collisional condition was assumed because the inside of cryopump is high vacuum condition as far as the temperature of the second stage is maintained around 20 K.

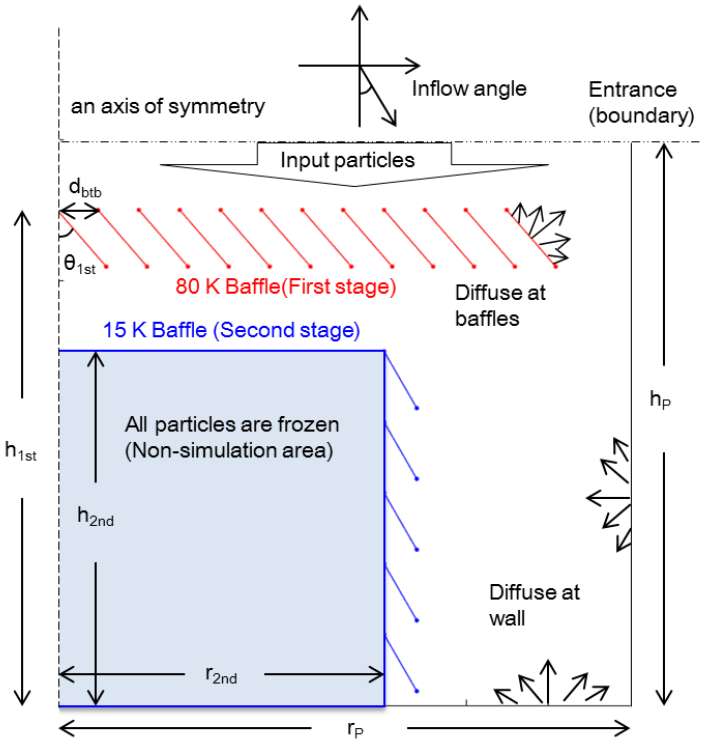

Figure 1. 2D3V simulation model of the axisymmetric two stage cryopump.

B. Results

The angle dependence of the calculated pump sticking coefficient is shown in the Fig. 2. Inflow angle means the vector angle of the inflow particles which shown in Fig. 1. The peak values of the pump sticking coefficient in both cases are around 35 degrees, which is reasonable because the slope of the baffle of this calculation is 36.87 degrees. When h_p is longer, at a larger angle than the peak, the pump coefficient is lower than short h_p. This is because that with the longer h_p, the probability of hitting to the second stage decreases with the increase of the collision of inflow

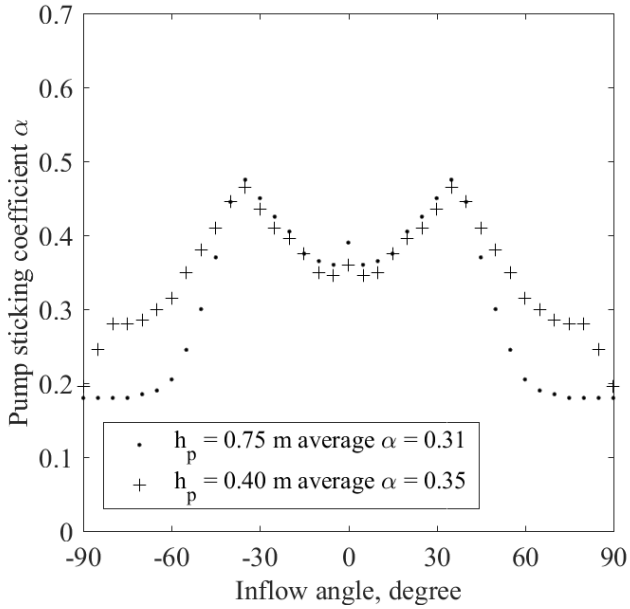

Figure 2. Simulation results of pump sticking coefficient vs. flow angle.

particles with the outer wall. The reason of the slight increase of the pump sticking coefficient near the 0 degrees is due to the increase of the ratio of flow which through the region without the baffle near the side wall and reach inside of the cryopump without hitting the side wall. Note that in this simulation the flows with angles crossing sections are not considered. Thus this angle dependency is not exactly applicable for cylindrical cryopump and three-dimensional simulation is required. However, it would be applicable for square type cryopump. The average pump sticking coefficients are 0.31 and 0.35 for h_p = 0.75 and 0.45, respectively. These average values are effective when the flow from the chamber to the cryopump can be regarded as random.

The relationship between the inflow angle and the angle of the velocity vector of the reflected particle leaving without being evacuated by the pump was investigated. The ratios of reflected particles at each inflow angle in Fig. 3 are normalized by the each maximum value. Since the model is an axisymmetric, the results of the 0 to -90 degrees of the inflow angle are axisymmetric with 0 to 90 degrees. The ratio is large at the opposite angle with respect to the inflow angle. This indicates that a lot of particles go out following the inverse of the trajectory of the inflow particles. Moreover, the ratio of reflected particles slightly increases around ± 30 degrees. The reason is because of the angle of the baffle at the first stage. It is concluded that the trajectory of the reflected particles has a dependency on the inflow angle. The more accurate particle trajectory can be calculated by modeling this angle dependency of reflected particles.

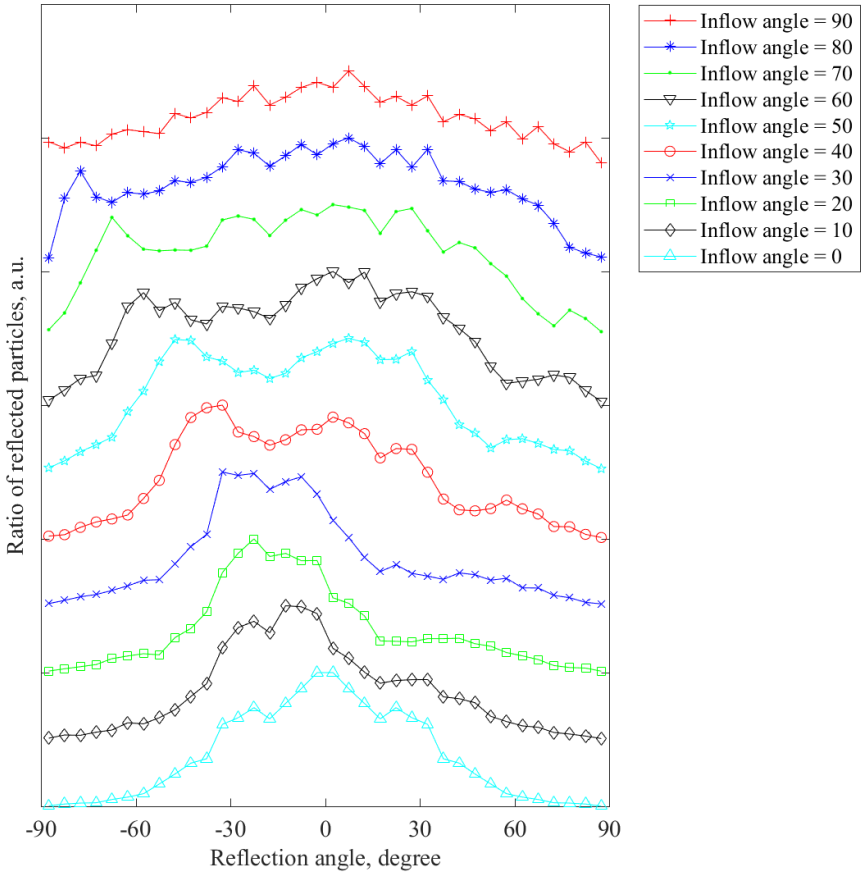

Figure 3. Simulation results of the ratio of reflected particles vs. reflection angle with different Inflow angles.

III. 3D simulation inside vacuum chamber and pressure measurement

A. Three-dimensional particle simulation of the IHI vacuum chamber

The motion of the particles inside the IHI vacuum chamber was calculated by using DSMC. The schematic of the simulation model is shown in Fig. 4. Calculated particles were xenon neutrals and input from the inlet set at 0.3 m from the upstream of the chamber. The inflow port was an annular section with the inner diameter of 4.35 mm

modeling a quarter inch pipe. Input mass flow rate was 4 mg/s and their velocity were determined to satisfy the Maxwell-Boltzmann distribution depending on the temperature. In this model, thermal equilibrium in the chamber was assumed, and the calculated particle temperature and the chamber wall temperature were all given at room temperature of 300 K. All particles were diffused with thermal velocity on the wall. Two cryopumps were installed one on each side of the chamber wall with different diameter. In the IHI vacuum chamber, the cryopump is installed at the end of the cylindrical pipe, and thus the pump sticking coefficient $\alpha = 0.31$ of longer h_p is adopted. The particles arriving at the cryopump area were either removed from the calculation or reflected under the same conditions as the wall surface according to the proportion of the pump sticking coefficient. Here, thermal exchange between the particles and the cryopump was not considered.

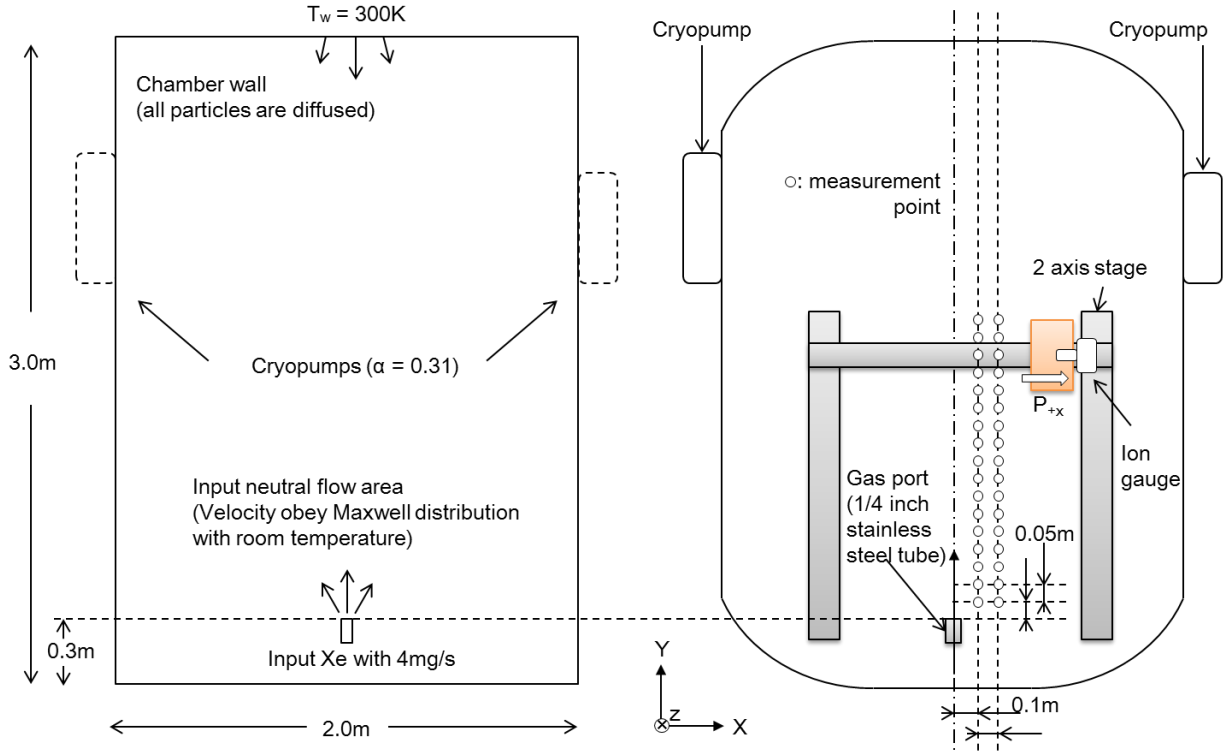

Figure 4. Schematics of cross-section of 3D simulation model and experiment in the IHI vacuum chamber.
The left figure is the schematic of simulation and right figure is the schematic of the pressure measurement.

B. Pressure measurement setup for the validation of the estimated pump sticking coefficient

In order to validate the simulation result with analytically obtained pump sticking coefficient, pressure distribution inside the IHI vacuum chamber was measured. The chamber was evacuated by two cylindrical cryopumps with keeping the temperature of the second stage below 20 K. The base pressure was achieved the order of 10^{-4} Pa. For the future pressure measurement with thruster operation plasma, the ionization gauge was mounted on a neutralizer recommended by Dankanich et at.[17] The neutralizer is constituted with stainless steel pipe and the diameter of the entrance is 23 mm. The ionization gauge was mounted on the two-axis positioning stage. The entrance of the neutralizer faced the -X direction and the total pressure in the + X direction was measured. Fig. 4 displays the 0.5 m by 0.5 m square grid on which data points were taken. Input mass flow was the same as simulation condition, 4 mg/s for xenon. The inflow port was a quarter pipe and set at 0.3 m from the upstream of the chamber.

C. Results and discussion

The calculation of the total pressure in the + X direction in numerical simulation was carried out by the following method. The flux F_i flowing across a certain surface is calculated by counting total particles flowing from one section of a cell box as shown in Fig. 5. Here, flux density Φ_i is obtained by F_i. At the entrance of the neutralizer, the incoming flux density Φ_{into_n} and the outgoing flux density are in equilibrium under the steady state condition.

By assuming that the thermal equilibrium is established by the collision of the neutralizer and particles, Φ_{into_n} is expressed as

$$\Phi_{into\_n} = \frac{1}{4} n_n \sqrt{8 k_B T_n / \pi m} \tag{1}$$

where k_B is Boltzmann's constant, m is molecular mass of xenon, n_n is the number density inside the neutralizer and T_n is the temperature of the neutralizer. The pressure which ionization gauge indicates is proportional to the number density of the measured area. Thus, P_{+x} is expressed by following ideal gas equation.

$$P_{+x} = n_n \times k_B T_n \tag{2}$$

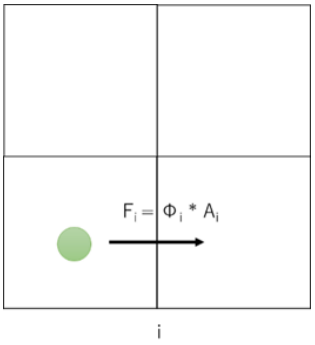

Figure 5. Image of counting flux across the cell boundary.

The comparison of measured and calculated pressure distribution in IHI vacuum chamber is shown in Fig. 6. Corrected pressure P_c of xenon in the measurement is expressed as

$$P_c = \frac{P_i - P_b}{2.87} + P_b \tag{3}$$

where P_b is base pressure and P_i is indicated pressure. The measured base pressure was 3×10^{-4} Pa. Vender specified accuracy is ±15 %, however, 30-50 % total uncertainty has been historically demonstrated because there are errors caused by various factors such as a flow meter, position and voltage signal recorder.[17] On-site calibration of the ionization gauge is not carried out. The error bar on the graph indicates ±30% of the measured pressure. When estimating pump sticking coefficients from experimental data considering error bars, the range is 0.35 to 0.21. The simulation results with analytically estimated pump sticking coefficient agree with the experimental results within ±30%. There is a possibility that the number density inside the neutralizer distributed due to the influence of ionized particles. Due to the non-equilibrium distribution, calculated pressure may be underestimated. This method which can determine the pump sticking coefficient without experimental information is useful for the design of vacuum facility. Moreover, by reducing the tuning parameters in numerical simulation, the value of other parameters can be discussed.

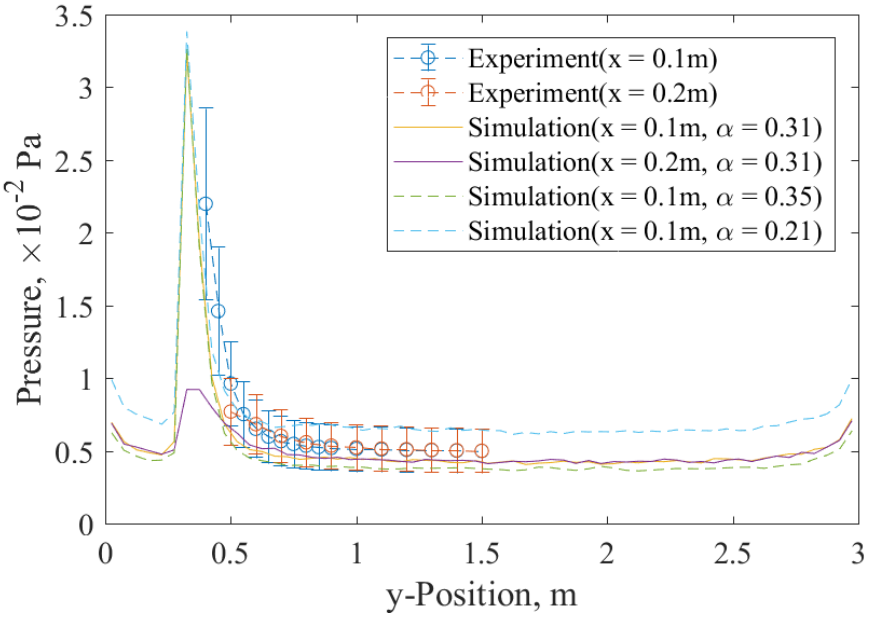

Figure 6. Results of measured and calculated pressure distribution.

IV. Estimation of the ingestion mass flow rate

A. Simulation model

We created the three-dimensional simulation model of a large vacuum chamber referring to the work of Nakayama.[18] The schematic of the model is shown in Fig. 7. The chamber is 3 m in diameter by 9 m length, evacuated by 21 cryopumps which the diameter is 0.75 m. Seven pumps are equally installed circumferentially at positions 1.5, 3, and 4.5 m from the downstream, respectively. The specifications of the assumed 600 mN class thruster are shown in the table 1. The biggest difference compared to the work by Nakayama was the handling of inflowing particles. Inflowing particles were set as single ions and neutral particles according to the propellant utilization efficiency. The single ions were accelerated with an acceleration voltage and injected from an annular section, assuming a thruster according to the divergence angle. The rest of the propellant was injected as the neutral with thermal velocity of room temperature. Any effect to ions from external force such as the electric field was not considered, and only the orbit is calculated. When a single ion hit the chamber target or wall surface, it becomes a neutral particle. Single ions were diffused or reflected specular on the wall according to the ratio of the diffusion and specular reflection and here this ratio was set to 0.5. Single ions were not evacuated by cryopumps. The handling of neutral particles was the same as the simulation of the IHI vacuum chamber shown in the section III. Pump sticking coefficient was set to 0.31. Two target configurations, the conical target and flat target, were modeled to investigate the differences. The angle of the conical target θ_{ta} was set to 26.6 degrees so that the particle which incidents to the most downstream pump was maximized. The edge of the conical target is located 0.1 m inside the chamber edge in order to avoid locally increasing the reflection of particles and walls in a narrow area. In this simulation, any beam dumper or shield was not assumed. The only collision that was considered was the elastic collision between the neutrals. The difference between the neutral velocity and ion velocity is large enough to consider that an ion-neutral elastic collisional cross section more than an order of magnitude smaller than the cross section of the elastic collisions between neutrals. Thus, ion-neutral elastic collision was ignored. Charge exchange between ions and neutrals was also not considered. If the charge exchange is considered, the ingestion mass flow rate would possibly be decreased.

Table 1. The specifications of the assumed Hall thruster.

Parameter	Value
Propellant	Xe
Propellant utilization efficiency, %	85
Beam divergence angle, degree	40
Outer diameter of the discharge chamber, m	0.45
Width of the discharge chamber, m	0.035
Acceleration voltage, V	300

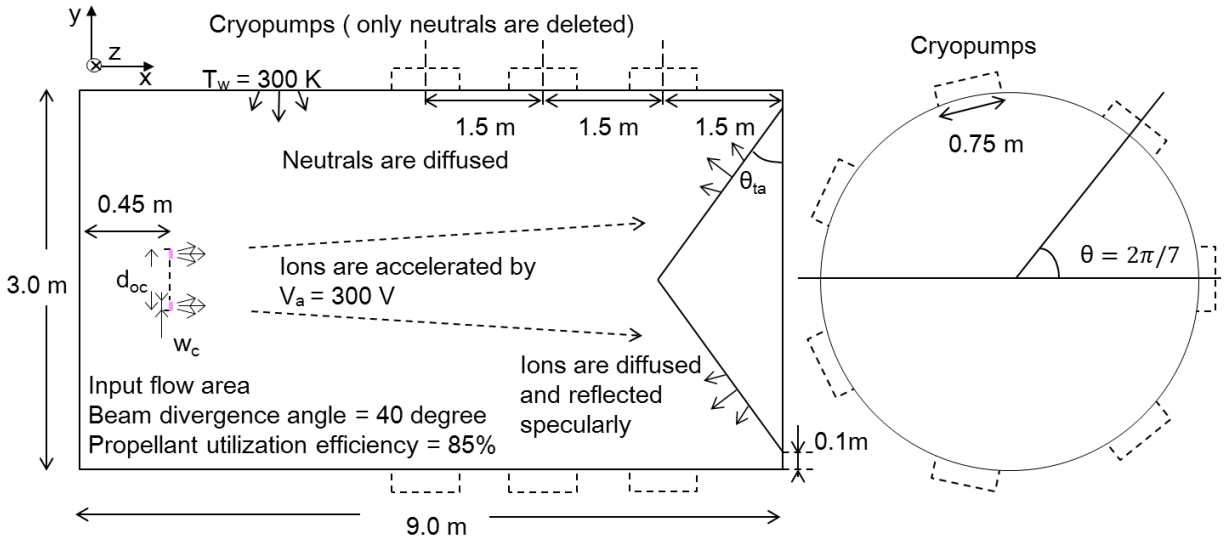

Figure 7. Schematic of the 3D simulation model of the φ 3m × 9 m vacuum chamber.
The left figure is the schematic cross-section and the right figure is the schematic of the front view

B. Result

The simulation results with different target configuration are shown in the table 2. In order to investigate the difference between high pressure condition and low pressure condition, two anode mass flow rate case m_a = 40 mg/s and m_a = 5 mg/s were calculated. From the particle motion analysis, the number of reflections and the number of collisions experienced before particles were evacuated were counted. Even in a large chamber with low anode mass flow rate case, the average number of reflections exceeds several tens of times. This is because of the fact that the proportion of the total surface area of cryopumps to the surface area of the chamber wall is 11 % although 21 cryopumps were installed in the chamber. The ingestion mass flow rate was estimated by counting the particles which entered the annular surface assuming the discharge chamber of a Hall thruster. In the low anode mass flow case, ingestion mass flow rate under the conical target configuration was less than that under the flat target configuration. On the other hand, in the high anode mass flow rate case, ingestion mass flow rate was not affected by the target shape.

Table 2. Simulation results.

Input	Anode mass flow rate, mg/s	40		5	
	Target shape	Flat	Conical	Flat	Conical
Output	Number of reflection	30	33	31	27
	Number of collision	107	117	18	15
	Ingestion mass flow rate, mg/s	0.82	0.80	0.11	0.10
	Ratio of ingestion and anode mass flow rate	2.0%	2.0%	2.2%	2.0%

C. Discussion

The distributions of the particles to the chamber wall after ions were neutralized on the target or the chamber wall were counted and are shown in Fig. 8. Only the neutrals immediately after neutralization of ions were counted. In the case of m_a = 5 mg/s, the clear difference in the distribution of the particles is observed around x = 7 to 9 m.

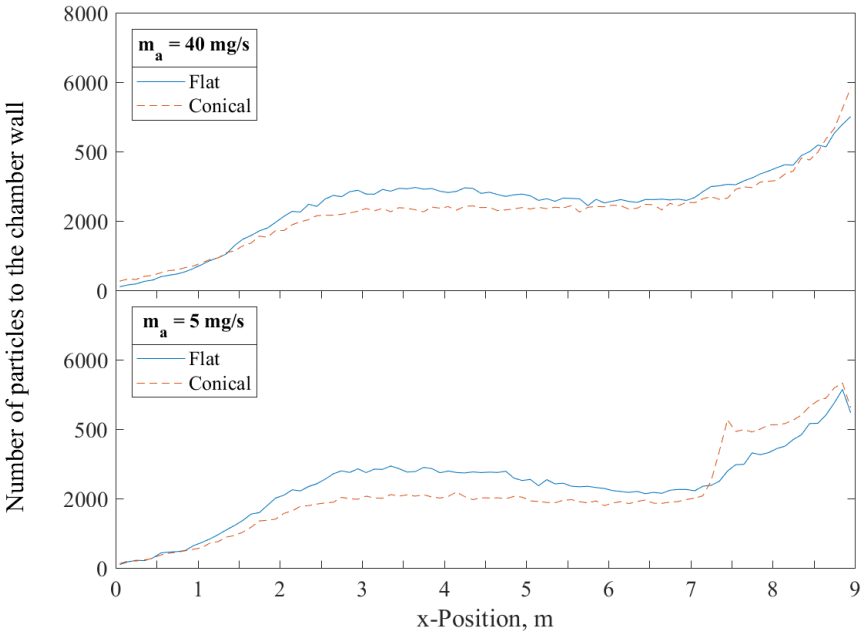

Figure 8. Distributions of the particles to the chamber wall.
The top figure is the case of m_a = 40 mg/s and the bottom figure is the case of m_a = 5 mg/s. Only the neutrals immediately after neutralization of ions were counted.

This indicates that the target produced the flow of particles as expected. On the other hand, in the case of m_a = 40 mg/s, any significant difference is observed in the distribution of the particles. As a result, the motions of the particles inside the chamber were same and any change could not be appeared between the conical target and flat target. Many numbers of neutral collisions suggest that because of the relatively high pressure inside the chamber, the flow from the target was disturbed. This study indicates that the conical target would be able to reduce ingestion mass flow rate when the particles motion could be treated as collision-less. However, the reduction of the ingestion mass flow rate was small in this simulation. It is necessary to optimize the pump position and target shape considering the beam divergence angle of the thruster. Note that the ratio of diffusion and specular reflection of ions on the wall was set to 0.5 in this simulation and if diffusion is more dominant, the effect of the target shape would decrease.

V. Conclusion

In order to establish the accurate prediction method of the ingestion mass flow rate, pump sticking coefficient was analytically estimated. In the cryopump consisting of two-stage structure, xenon particles are reflected on the first stage, and the pumping speed depends on the transmittance of the first stage. Therefore, the pump sticking coefficient can be estimated by the proportion of the amount of particles captured by the second low temperature stage to the amount of particles flowing into the cryopump. The pump sticking coefficient varies depending on the inflow angle of the particles. Moreover, it was indicated that the flow of the reflected particles also depends on the inflow angle. In this research, the flows with angles crossing sections were not considered. For more accurate simulation of the inflow angle dependency, three-dimensional simulation is necessary. The average pump sticking coefficients were estimated for both the case with long height assuming the cryopump installed to the cylinder pipe and the case with short height. The estimated average pump sticking coefficients were 0.31 and 0.35 for h_p = 0.75 and 0.45, respectively.

The validation of the estimated pump sticking coefficient was conducted by the comparison between simulation and measurement of the pressure distribution of IHI vacuum chamber. The average pump sticking coefficient α = 0.31 was used to the simulation. Measured and simulated pressure distributions were consistent within the range of ± 30%. The cause of the difference is considered that because the non-equilibrium distribution was created by ionized particles, calculated pressure was possibly underestimated. However, this method can determine the pump sticking coefficient without experimental information and it is useful for the accurate prediction of the particle motion inside the chamber. In addition, other simulation parameters can be investigated by reducing the parameter which is determined empirically.

Finally, three-dimensional simulation model of the φ 3m × 9 m vacuum chamber was developed. By the estimation of the ingestion mass flow rate assuming 600 mN class Hall thruster operation, the effect of the target shape to the ingestion mass flow rate was investigated. Two cases with different target shape were simulated, flat and conical. The angle of the conical target was set based on the concept of increasing the inflow particles to the most downstream pump. Anode mass flow was set as input parameter. Although the reduction of the ingestion mass flow rate by the conical target was observed in the low anode mass flow case, ingestion mass flow rate was not affected by the target shape in the high anode mass flow rate case. Because the number of collisions between neutrals was more than a hundred, the flow from the conical target was disturbed in the high anode mass flow rate case. It is suggested that the conical target would be able to reduce ingestion mass flow rate when the particles motion could be treated as collision-less. However, to reduce the ingestion mass flow by the target, it is necessary to optimize the pump position and target shape considering the beam divergence angle of the thruster.

References

[1]Mitsubishi Electric Corporation, "Mitsubishi Electric Chosen as Prime Contractor of Japanese Government's Engineering Test Satellite 9", No.3095, Apr.2017, URL: http://www.mitsubishielectric.com/news/2017/0407-a.html [cited 7 April 2007].

[2]Hamada, Y., Bak, J., Kawashima, R., Koizumi, H., Komurasaki, K., Yamamoto, N., Egawa, Y., Funaki, I., Iihara, S., Cho, S., Kubota, K., Watababe, H., Fuchigami, K., Tashiro, Y., Takahata, Y., Kakuma, T., Furukubo, Y., and Tahara, H., "Hall Thruster Development for Japanese Space Propulsion Programs," *Transactions of JSASS*., Vol. 60, No. 5, pp. 320-326, 2017.

[3]Yamamoto, N., Miyasaka, T., Komurasaki, K., Koizumi, H., Schoenherr, T., Tahara, H., Takegahara, H., Aoyagi, J., Nakano, M., Funaki, I., Watanabe, H., Ohkawa, Y., Kakami, A., Takao, Y., Yokota, S., Ozaki, T., and Osuga, H., "Developments of Robust Anode-layer Intelligent Thruster for Japan IN-space propulsion system," *33rd International Electric Propulsion Conference*, IEPC-2013-244, 2013.

[4]Funaki, I., Iihara, S., Cho, S., Kubota, K., Watanabe, H., Fuchigami, K., and Tashiro, Y., "Laboratory Testing of Hall Thrusters for All-electric Propulsion Satellite and Deep Space Explorers," *52nd Joint Propulsion Conference*, AIAA 2016-4942, 2016.

[5]Frieman, J. D., King, S. T., Walker, M. L. R., Khayms, V., and King, D. Q., "Role of a Conducting Vacuum Chamber in the Hall Effect Thruster Electrical Circuit," *Journal of Propulsion and Power*, Vol. 30, No. 6, pp. 1471-1479, 2014.

[6]Byers, D., and Dankanich, J. W., "A review of facility effects on Hall effect thrusters." *31st International Electric Propulsion Conference*, IEPC-2009-076, 2009.

[7]Frieman, J. D., Walker, J. A., Walker, M. L. R., Khayms, V., and King, D. Q., "Electrical Facility Effects on Hall Thruster Cathode Coupling: Performance and Plume Properties." *Journal of Propulsion and Power* Vol. 32, No. 1, pp. 251-264, 2016.

[8]Yim, J. T., Burt, J. M., "Characterization of Vacuum Facility Background Gas Through Simulation and Considerations for Electric Propulsion Ground Testing," *51st AIAA/SAE/ASEE Joint Propulsion conference*, AIAA 2015-3825, 2015.

[9]Walker, M. L. R., and Gallimore, A. D., "Neutral density map of Hall thruster plume expansion in a vacuum chamber," *Review of Scientific Instruments*, Vol. 76, No. 5, pp. 1-10, 2005.

[10]Walker, M. L. R., Victor, A. L., and Hofer, R. R., "Gallimore, Alec D.Effect of Backpressure on Ion Current Density Measurements in Hall Thruster Plumes, " *Journal of Propulsion and Power*, Vol. 21, No. 3, pp. 408-415, 2005.

[11]Diamant, K. D., Liang, R., and Corey, R. L., "The Effect of Background Pressure on SPT-100 Hall Thruster Performance," *50th AIAA/ASME/SAE/ASEE Joint Propulsion Conference*, AIAA 2014-3710, 2014.

[12]Brown, D. L., "Investigation of low discharge voltage Hall thruster characteristics and evaluation of loss mechanisms," Ph.D. Dissertation, Aerospace Engineering Dept., Univ. of Michigan, Ann Arbor, MI, 2009.

[13]Huang, W., Kamhawi, H., and Haag, T., "Facility Effect Characterization Test of NASA's HERMeS Hall Thruster," *52nd AIAA/SAE/ASEE Joint Propulsion Conference*, AIAA 2016-4828, 2016.

[14]Cai, C., "Theoretical and Numerical Studies of Plume Flows in Vacuum Chambers," Ph.D. Dissertation, Aerospace Engineering Dept., Univ. of Michigan, Ann Arbor, MI, 2005.

[15]Frieman, J. D., Liu, T. M., and Walker, M. L. R., "Background Flow Model of Hall Thruster Neutral Ingestion," *Journal of Propulsion and Power*, Vol. 33, No. 5, pp. 1087-1101, 2017.

[16]Nakayama,Y., and Nakamura, M., "Electric Propulsion Propellant Flow within Vacuum Chamber," *34th International Electric Propulsion Conference*, IEPC 2015-360, 2015.

[17]Dankanich, J. W., Walker, M. L. R., Swiatek, M. W., and Yim, J. T., "Recommended Practice for Pressure Measurement and Calculation of Effective Pumping Speed in Electric Propulsion Testing," *33rd International Electric Propulsion Conference*, IEPC 2013-358, 2013.

[18]Nakayama, Y., "Propellant Flow Analysis within Electric Propulsion Test Facility," *31st International Symposium on Space Technology and Science*, ISTS 2017-b-18, 2017.